Molecular Vision 2014; 20:1695-1709 <http://www.molvis.org/molvis/v20/1695>
Received 11 September 2014 | Accepted 18 December 2014 | Published 20 December 2014

© 2014 Molecular Vision

Disease progression in iridocorneal angle tissues of BMP2-induced ocular hypertensive mice with optical coherence tomography

Guorong Li,[1] Sina Farsiu,[1,2] Jianming Qiu,[1] Angela Dixon,[1] Chunwei Song,[4] Stuart J. McKinnon,[1,3] Fan Yuan,[2] Pedro Gonzalez,[1] W. Daniel Stamer[1,2]

[1]Department of Ophthalmology, Duke University, Durham, NC; [2]Department of Biomedical Engineering, Duke University, Durham, NC; [3]Department of Neurobiology, Duke University, Durham, NC; [4]School of Astronautics, Harbin Institute of Technology, Harbin, China

Purpose: The goal of the present study was to test for the first time whether glaucomatous-like disease progression in a mouse can be assessed morphologically and functionally with spectral domain optical coherence tomography (SD-OCT).
Methods: We monitored progressive changes in conventional outflow tissues of living mice overexpressing human bone morphogenetic protein 2 (BMP2), a model for glaucoma. Intraocular pressure (IOP) and outflow tissue morphology/Young's modulus were followed in mice for 36 days with rebound tonometry and SD-OCT, respectively. Results were compared to standard histological methods. Outflow facility was calculated from flow measurements with direct cannulation of anterior chambers subjected to three sequential pressure steps.
Results: Overexpression of BMP2 significantly elevated IOP in a biphasic manner over time compared to mice that overexpressed green fluorescent protein in outflow cells and naïve controls. SD-OCT revealed changes in outflow tissues overexpressing BMP2 that corresponded with the timing of the IOP phases and decreased outflow facility. In the first phase, the angle was open, but the trabecular meshwork and the cornea were thickened. OCT detected increased trabecular meshwork stiffness after provocative IOP challenges of the BMP2 eyes, which corresponded to increased collagen deposition with transmission electron microscopy. In contrast, the angle was closed in the second phase. IOP elevation over 36 days due to BMP2 overexpression resulted in significant retinal ganglion cell and axon loss.
Conclusions: Although not a feasible open-angle glaucoma model, the BMP2 mice were useful for demonstrating the utility of SD-OCT in following disease progression and differentiating between two forms of ocular pathology over time that resulted in ocular hypertension.

Rodent models are valuable tools for studying neurodegenerative diseases. For years, rodent models for glaucoma have consisted of sclerosing, ablating, or clogging elements of the conventional outflow pathway to elevate intraocular pressure (IOP) and examine the mechanical and ischemic effects on retinal ganglion cell (RGC) viability. For example, IOP was elevated in rats by laser photocoagulation of episcleral veins [1], episcleral vein occlusion [2], and sclerosis of the trabecular meshwork (TM) by retrograde injection of hypertonic saline into episcleral veins [3]. Similar techniques were adapted to mice due to the advantages of genetic manipulation to study the function of critical genes and biochemical pathways. For instance, laser photocoagulation of mice episcleral veins induced transient elevation of IOP and loss of axons; however, there were complications such as corneal edema, corneal opacity, and cataract in the lasered eyes [4]. Moreover, episcleral vein occlusion in mice was induced by cauterization of three episcleral venous trunks, producing a sustained increase in IOP in a substantial portion of the treated mice [5]. Recently, IOP was significantly elevated in mice by intracameral injection of beads [6,7] or trabecular sclerosis following retrograde injection of hypertonic saline into the episcleral veins of mice [8]. Alternatively, the DBA/2J mouse sporadically develops ocular hypertension due to pigment dispersion and TM dysplasia and has been commonly used as a glaucoma model. DBA/2J mice provide a tractable model for dissecting the pathways of cell death in inherited glaucoma and the role of the immune system in mediating disease and investigating neuroprotective strategies [9-11].

Although suitable for examining IOP-dependent changes in retinal ganglion cell biology, such mouse models are not amenable for studying conventional outflow function, which is defective in ocular hypertensive patients. To better study outflow dysfunction, mouse models for ocular hypertension have become more sophisticated at genetically targeting cells in the conventional outflow tract. Recently, several mouse models of ocular hypertension were developed by

Correspondence to: W. Daniel Stamer Duke University DUMC 3802 Durham, NC 27710 Phone: (919) 684-3745; FAX: (919) 684-8983; email: dan.stamer@.duke.edu

targeting the conventional outflow pathway. For example, overexpression of mutant myocilin through introducing a disease-causing point mutation (Tyr437His) in transgenic mice [12] or intravitreal injection of adenovirus-encoding mutant myocilin in wild-type mice results in prolonged ocular hypertension (10–15 mmHg above control) [13]. In another model, overexpression of connective tissue growth factor (CTGF) in the crystalline lens of transgenic mice or by intracameral injection adenovirus encoding CTGF results in ocular hypertension. This model has modest (about 5 mmHg) but prolonged IOP elevation compared to control animals [14]. Transgenic mice ($Col1a1^{r/r}$) that had a targeted mutation in the gene for procollagen type Iα1 subunit also showed an increase in IOP (about 6 mmHg) at 36 weeks compared to the wild-type control mice ($Col1a1^{+/+}$) [15]. Last, overexpression of the active form of human transforming growth factor-β2 ($hTGF\beta2^{226/228}$) by intracameral or intravitreal injection of adenovirus encoding the cytokine into mouse eyes induces a sustained increase in IOP (about 8 mmHg) for 28 days, with a corresponding decrease in outflow facility [16]. Although each of these newer mouse models are ocular hypertensive, disease progression at the level of the conventional outflow pathway was primarily assessed with IOP measurements over time and standard morphological analysis at select time points. The exception was with the Col1a1 and TGF-β2 models, which detected compromised outflow function by measuring outflow facility in living mice [16,17].

Optical coherence tomography (OCT) [18] has proven to be an invaluable tool for evaluating retinal diseases in humans [19] and in mice [20]. Several recent studies have addressed the problem of imaging the conventional outflow pathway in human eyes using OCT [21-24]. However, imaging of the mouse conventional outflow pathway with OCT has different technical obstacles (i.e., small eye, blood in Schlemm's canal [SC], and the need for iridotomy to prevent anterior chamber deepening). Very recently, we modified a commercial OCT imaging system to study conventional outflow function in real time in living mice, and showed the role of ciliary muscle contraction in preventing IOP-induced collapse of SC [25]. The present study was designed to extend these observations and monitor the impact of genetic changes on the conventional outflow tract of mice on its morphology and function with OCT. Here we utilize engineered adenovirus that encodes bone morphogenetic protein-2 (BMP2), a member of the TGF-β superfamily [26], for targeted overexpression in conventional outflow tissues to elevate IOP in mice. The rationale for using BMP2 here is that BMP2 ligands and TGF-β2 have the ability to signal via canonical and non-canonical pathways and TM cells have the capacity to use both pathways [27]. In addition, BMP2 involves calcification in cultured human TM [28] and induced ocular hypertension in rats without altering the structure of the outflow tissues [29]. We hypothesized that overexpression of BMP2 in outflow tissues might also induce elevated IOP and the disease progression in outflow tissues may be resolved with OCT.

METHODS

Experimental SD-OCT setup, image processing, and segmentation: In vivo imaging was performed utilizing an Envisu S4110-XHR extreme-high-resolution SD-OCT system (Bioptigen Inc., Research Triangle Park, NC). The Bioptigen S4110 XHR SD-OCT used for this study included the NKT Super K Extreme super-continuum light source, model EXR-1. The output of the source light was coupled into Bioptigen's proprietary OCT design, which includes a custom wave number linear grating spectrometer. The final typical output power from the SD-OCT is 1 mW over the 670–970 nm bandwidth. Mice were infused with Ad.cmv. BMP2 or Ad.cmv.GFP and imaged at different time points after the viral infusion. To prevent anterior chamber deepening, iridotomy was conducted around 1 week before the OCT imaging sessions (after the viral infusions) as described previously [25]. For OCT experiments at the 1 week time point, iridotomy was conducted 1 day after the viral infusion to prevent anterior chamber deepening during single needle perfusions. Mice were anesthetized as before, and then placed on a custom-made OCT imaging mount that we designed and manufactured specifically for imaging mice. The mice were anesthetized with an intraperitoneal injection of ketamine (100 mg/kg) and xylazine (10 mg/kg).A drop of 0.5% proparacaine, a topical anesthetic, was applied to the eye to be imaged. Using a micromanipulator connected to an imaging mount, a pulled glass microneedle was filled with PBS (1X; 137 mM NaCl, 2.7 mM KCl, 8 mM Na_2HPO_4, and 2 mM KH_2PO_4, pH 7.4) and inserted into the mouse anterior chamber. The microneedle was connected to a manometric column to adjust the IOP and a pressure transducer to continuously monitor IOP levels (using PowerLab software). The OCT probe was aimed at the inferior lateral limbus, and the image was centered and focused at SC. While images were collected in the same SC region, the mouse eye was subjected to a series of IOP steps (10, 15, 20, 25, 30, 35, and 45 mmHg) by adjusting the height of a fluid reservoir. At each IOP step, a sequence of repeated OCT B-scans (each with 1000 A-scans spanning 1 mm in lateral length) from spatially very close positions was captured, registered, and averaged to create a high signal-to-noise-ratio image from the anterior segment of each animal. Image registration and SC lumen area analyses

were performed utilizing the ImageJ (freeware; National Institutes of Health, Bethesda, MA) StackReg registration plug-in [30]. Each averaged OCT image was opened into ImageJ software and SC area was manually marked and area calculated. Estimates of lumen borders were verified with the lumen edges observed in live video, comparing stationary lumen edges with moving reflectors (blood cells in lumen). Area calculations at each pressure level were normalized to the area of 10-mm Hg of each eye [25].

Animal experiments: Mice were handled in accordance with the animal care and use guidelines of the Institutional Animal Care and Use Committee of Duke University and in compliance with the ARVO Statement for the Use of Animals in Ophthalmic and Vision Research. CD1 wild-type mice were purchased from the Jackson Laboratory (Bar Harbor, ME), bred/housed in clear cages, and kept in housing rooms at 21 °C with a 12 h:12 h light-dark cycle. We chose non-pigmented CD1 mice so that the ciliary body could be visualized with OCT during the imaging sessions. A total of 74 mice (ages between 6 and 10 weeks old when the experiments began) were used in this study. Viral infusion and iridotomy were conducted at the Duke Eye Center animal facility, and other measurements were conducted in our laboratory for the end point measurement. To reduce the numbers, the animals were euthanized after IOP, OCT, and outflow facility measurements sessions so that the eyes could be also examined with standard histology for comparisons.

Adenoviral vectors: Adenovirus expressing human BMP2 driven by cytomegalovirus (CMV) promoter (Ad.cmv.BMP2) was purchased from Signagen Laboratories (Rockville, MD, Cat# SL101898). Adenovirus-expressing green fluorescence protein (Ad.cmv.GFP) was constructed and characterized in our laboratory using the ViraPower Adenoviral Expression System (Invitrogen, Grand Island, NY) as described previously in a study [31]. Both viruses were grown and amplified in HEK293 cell lines. The viruses were further purified and titered using the Adenovirus Mini purification ViraKit (VIRAPUR, San Diego, CA) and the Adeno-X Rapid Titer kit (Clontech Laboratories, Mountain View, CA) following the manufacturer's instructions.

Intracameral infusion of Ad.cmv.BMP2 and Ad.cmv.GFP: Intracameral infusion of the virus was performed as previously described using Ad.cmv.GFP to monitor gene delivery and optimize the conditions for specifically targeting conventional outflow cells, largely not transducing surrounding iridocorneal cells [31]. The mice were anesthetized with an intraperitoneal injection of ketamine (100 mg/kg) and xylazine (10 mg/kg). A drop of 0.5% proparacaine, a topical anesthetic, was applied to the eyes. A pulled microglass needle filled with either Ad.cmv.BMP2 or Ad.cmv.GFP and connected to a pump was inserted in one of the mouse anterior chambers (another non-treated eye was used as the control either for BMP2 or green fluorescent protein [GFP]). Five microliters of viral solution containing 5×10^7 viral particles was infused in the mouse anterior chambers at a rate of 1.7 µl/min. This protocol was optimized to avoid damaging ocular structures and specifically target conventional outflow tissues [31]. After infusion, the needle was withdrawn, and topical erythromycin antibiotic ointment was applied to the infused eyes. The mice were maintained on a warm water-circulating blanket until they had recovered from the anesthesia.

RNA isolation and Q-PCR analysis of BMP2 gene expression: Mouse outflow tissues (TM/SC) from the virus-transduced eyes and the contralateral control eyes were carefully dissected from anterior segments of the bisected mouse eyes and placed in RNAlater (Sigma, St. Louis, MO) 3, 7, and 14 days after the Ad.cmv.BMP2 infusion. Total RNAs were isolated using the mirVana miRNA Isolation Kit (Cat#1560, Ambion, Grand Island, NY). RNA yields were measured using fluorescent dye (RiboGreen; Molecular Probes, Eugene, OR). First-strand cDNA was synthesized from total RNA (100 ng) with reverse transcription using oligo-dT and reverse transcriptase (Superscript III; Invitrogen Corporation) in a 10 µl volume. Quantitative real-time polymerase chain reaction (Q-PCR) was performed in a 20 µl mixture that contained 1 µl cDNA preparation and 1× real-time PCR mix (iQ SYBR Green SuperMix; Bio-Rad, Hercules, CA) using the following PCR parameters: 95 °C for 3 min followed by 40 cycles of 95 °C for 10 s, 60 °C for 30 s followed by a melt curve (65 °C–95 °C in increments of 0.5 °C for 5 s). Each quantification was conducted in duplicate, and the experiments were conducted in triplicate. The fluorescence threshold value (C_t) was calculated using real-time detection system software (iCycle; Bio-Rad). The absence of nonspecific products was confirmed with the analysis of the melt curves to exclude primer-dimer and with electrophoresis in gels (3% Super AcrylAgarose; Bio-Rad) to verify the correct product size. Mouse β-actin was used as an internal standard for mRNA expression to normalize the individual gene expression level. The specific primer pairs used to amplify the genes were as follows: human BMP2 forward primer (5′-CCC ACT TGG AGG AGA AAC AA-3′) and reverse primer (5′-GCT GTT TGT GTT TGG CTT GA-3′); mouse β-Actin forward primer: (5′-TCT TGG GTA TGG AAT CCT GTG GCA-3′) and reverse primer (5′-TCT CCT TCT GCA TCC TGT CAG CAA-3′).

IOP measurements: IOP was measured twice a week at the same time of day in the sedated mice using rebound

tonometry (TonoLab). Briefly, the mice were anesthetized with ketamine (60 mg/kg) and xylazine (6 mg/kg). IOP was measured immediately after the onset of anesthesia (light sleep). Each recorded IOP was the average of six measurements from the same eye. The IOP integral (on mmHg days), defined as the accumulation of IOP between the last measurement day (day 36) and the first measurement (day 0), was calculated.

Histology: Mouse eyes infused with Ad.cmv.BMP2 or non-infused contralateral eyes at 7 and 36 days were collected and immersed in fixative solution (2% paraformaldehyde plus 0.5% glutaraldehyde) overnight at 4 °C. The eyes were bisected, and the posterior segments and lens were removed. The anterior segments were cut into four quadrants, and each quadrant was embedded in Epon. Blocks were cut into 0.5 µm semithin sections and stained with 1% methylene blue. The images were captured digitally using light microscopy (Axioplan2, Carl Zeiss MicroImaging, Thornwood, NY). The 65 nm thin sections were stained with uranyl acetate/lead citrate and examined with electron microscopy (JEM-1400; JEOL USA, Peabody, MA).

Retinal ganglion cell and optic nerve axon counts: To count the RGCs in the retina flatmounts, the eyes infused with Ad.cmv.BMP2 (36 days) and the non-infused contralateral eyes were fixed with 4% paraformaldehyde overnight. The eyes were then bisected, and the retinas were stained with goat anti-mouse Brn3a antibody (1:750 dilution, Santa Cruz Biotechnologies, Santa Cruz, CA) and anti-goat immunoglobulin G (IgG; H+L) Alexa Fluor 568 (1:500 dilution, Molecular Probes). The retinas were then cut into center-connected four quadrants, flatmounted, and imaged from the center to the peripheral retina of the four quadrants using an EZ-C1.3.10 Nikon confocal microscope (20× lens) (D-ECLIPSE C1, Nikon). Each quadrant can hold three continuous images from the center (the optic nerve) to the peripheral retina. The third image (the peripheral retina) was used to count RGCs. Four peripheral retina images from each retina were used. The peripheral RGCs were counted using custom semiautomatic MATLAB-based software with a graphical user interface (GUI). The automatic algorithm first reduced the noise using an anisotropic filter [32]. Then, we used an iterative thresholding and watershed algorithm to segment the cells. Due to image artifacts, this automatic segmentation did not always result in perfect segmentation. Thus, an expert grader carefully reviewed the images and manually corrected all incorrectly segmented cells using the GUI of our software.

For optic nerve axon counts, we followed procedures previously described [33]. Briefly, optic nerves from the Ad.cmv.BMP2 eyes (36 days) or non-infused contralateral eyes were fixed (4% paraformaldehyde, 1% glutaraldehyde, and 0.12 M phosphate buffer) overnight. The samples were processed and embedded in the Embed-812 resin mixture. Blocks were sectioned on an ultramicrotome (LKB Ultratome V; Leica, Paris, France) using a glass knife. Cross sections were stained with 1% toluidine blue and coverslipped. Axon counts were obtained using the AxioVision imaging system (Zeiss). Image analysis consisted of RGB thresholding, followed by size and form factor exclusions. Approximately 40% of the total cross-sectional area for each optic nerve was counted, and the results were extrapolated to the entire nerve for each mouse.

Outflow facility and IOP measurement with direct cannulation: Outflow facility measurements were conducted in living mouse eyes as previously described by Camras [34] and modified by us [31]. Briefly, for bilateral measurements two micropipette manipulators were used to place a microneedle in each mouse eye. Each microneedle was connected to a pressure tubing (0.05 inch inner diameter, Mallinckrodt, Hazelwood, MO) leading to a three-way stopcock. The stopcock was connected to a 5 ml syringe filled with PBS and to pressure tubing connected to a second three-way stopcock. A pressure transducer (Honeywell model 142PC05D, Honeywell Sensing and Control, Golden Valley, MN) and a vertical column of fluid (RenaPulse Tubing 0.08 mm ID, Braintree Scientific Inc., Braintree, MA) were connected to the second stopcock. The transducer was connected to a PowerLab data acquisition system (ML870/P PowerLab 8/30, ADInstruments, Colorado Springs, CO) linked to a computer running PowerLab software. One glass column (0.05 mm ID, Sulter Instrument Co., Novato, CA) was connected to the top of the vertical pressure tubing to ensure that the liquid was vertical and the inner diameter was uniform for outflow calculations. The height of the fluid in the column was adjusted using a fluid-filled syringe. Transducers were calibrated before each experiment to ensure accurate pressure measurements. The height of the fluid of the column set the pressure in the system. The fluid exiting the system was proportional to the decline in the height of the column over time, and thus was used to determine the flow rate based on the dimensions of the fluid column. The average pressure over about 30 min was used due to the slight decline in pressure over time. Before the needle was inserted in the anterior chamber, pressure transducers were zeroed in the tear film. Initial IOP was recorded as soon as the needle entered the eye. Under the stereo microscope, care was taken to make sure no leak was observed around the needle. Outflow facility data were excluded if the mouse died or leaking occurred during outflow facility measurements. Flow was measured at three pressures (about 17, 25, and 35 mmHg), a linear regression

analysis was performed, and the slopes of the pressure-flow relationships were compared between the paired control vs. BMP2 or control vs. GFP-treated eyes to determine the outflow facility. Separate animals were transduced with BMP2 or GFP to avoid bilateral injections in a single animal. This design included two control groups to compare to the BMP2 transduced eyes, uninjected control eyes and GFP transduced eyes. The latter was important to control for the protein load in the transduced cells.

Estimation of Young's modulus of the TM: Our data here and previously [25] showed that the SC lumen decreased with increasing IOP in living mouse eyes. The decrease was presumably due to TM movement and deformation in response to the increase in IOP as observed in human eyes [35,36]; and the extent of the TM deformation depends on stiffness (E). To estimate this parameter, we made the following assumptions: (a) The SC lumen decrease was caused mainly by TM deformation, i.e., deformation of other tissues surrounding SC and the TM was negligible; (b) there was no change in the width of SC (long axis); (c) the pressure inside SC (P_{SC}) was approximately independent of IOP; and (d) the TM was a linear elastic material when TM deformation was small. Based on these assumptions, E can be estimated using Equation 1 [36]:

$$y = 100(1 - \frac{IOP - P_{sc}}{E} \rightarrow)$$

where y is the percentage of the cross-sectional area of SC relative to that with no pressure difference across the TM. To make sure that the TM deformation was very small, we used Equation 1 to fit the experimental data obtained with IOP varying only between 10 and 25 mmHg in mice in which the iridocorneal angle was open. To make sure that the positioning of the OCT probe was consistent between animals for these measurements, we gathered one to two OCT volumes containing SC at the inferior lateral limbus at least three clock hours away from the iridotomy site. The negative slope of the linear regression of y on the IOP was 100/E.

Statistical analysis

Statistical significance test of means between each group was assessed with single-factor ANOVA and the Student *t* test. A value of $p<0.05$ was considered statistically significant.

RESULTS

Characterization of living mice that overexpress BMP2 in conventional outflow tissues: Intracameral injection of Ad.cmv.BMP2 elevates IOP in rats [29]. To establish a mouse model of elevated IOP that could be followed over time with OCT, we transduced outflow cells by intracameral infusion of Ad.cmv.BMP2 (5×10^7 viral particles) using previously described methods we developed that selectively target outflow cells [31]. Instead of the monophasic IOP elevation observed in rats, we found that overexpression of BMP2 by TM cells elevated IOP in a biphasic pattern. As shown in Figure 1A, the IOP measured with TonoLab was significantly increased within 3 days after infusion of Ad.cmv.BMP2, peaking around 10 days (about 40 mmHg), and then dropping to about 20 mmHg at 14 days. Interestingly, the IOP then began to increase again to about 25–30 mmHg after 16 days for more than 20 days. The IOP in the control eyes, the contralateral non-transduced eyes and the Ad.cmv.GFP infused eyes, remained between 11 and 16 mmHg at all time points tested. The IOP difference in the comparison of the BMP2 eyes and the GFP control eyes reached statistical significance at all time points except at 14 days, the time when the pressure returned to nearly normal levels after the first phase of IOP elevation. The comparison of the IOP integral over 36 days between groups is shown in Figure 1B. Transduced human BMP2 gene expression levels in mouse outflow tissues were also examined. As shown in Figure 2, dramatic elevation in human BMP2 RNA expression in TM tissue dissected from transduced mice was found within 1 week (about 20,000-fold) and returned to normal levels at 2 weeks (about 70-fold), which is consistent with the observed IOP elevation at early time points and the decrease after 2 weeks. Due to visible changes in the cornea of the BMP2 transduced mice (peripheral corneal edema), we tested the IOP at three important time points (days 7, 14, and 36) by direct cannulation of the mouse anterior chambers. As shown in Figure 1, TonoLab appeared to overestimate the IOP by about 20 mmHg at day 7, was equivalent at day 14, and overestimated the IOP by about 10 mmHg at day 36 for the eyes transduced with BMP2. The TonoLab and direct cannulation measurements of the GFP eyes were nearly identical at all three time points (Figure 1A). Regardless, while less dramatic, a similar biphasic pattern of IOP elevation was observed using the direct cannulation method for measuring the IOP, and importantly, the IOP was significantly different at days 7 and 36. Moreover, the results are consistent with a specific effect of BMP2 but not the GFP virus on the cornea, particularly during the first week.

To test whether increased IOP in BMP2-transduced mouse eyes was caused by dysfunction of conventional outflow tissues, outflow facility was measured in the living mouse eyes after intracameral infusion of Ad.cmv.BMP2 or Ad.cmv.GFP and compared to the non-transduced contralateral eyes. Outflow facility was measured in living mice at day 7, the time of maximum IOP elevation, BMP2 overexpression

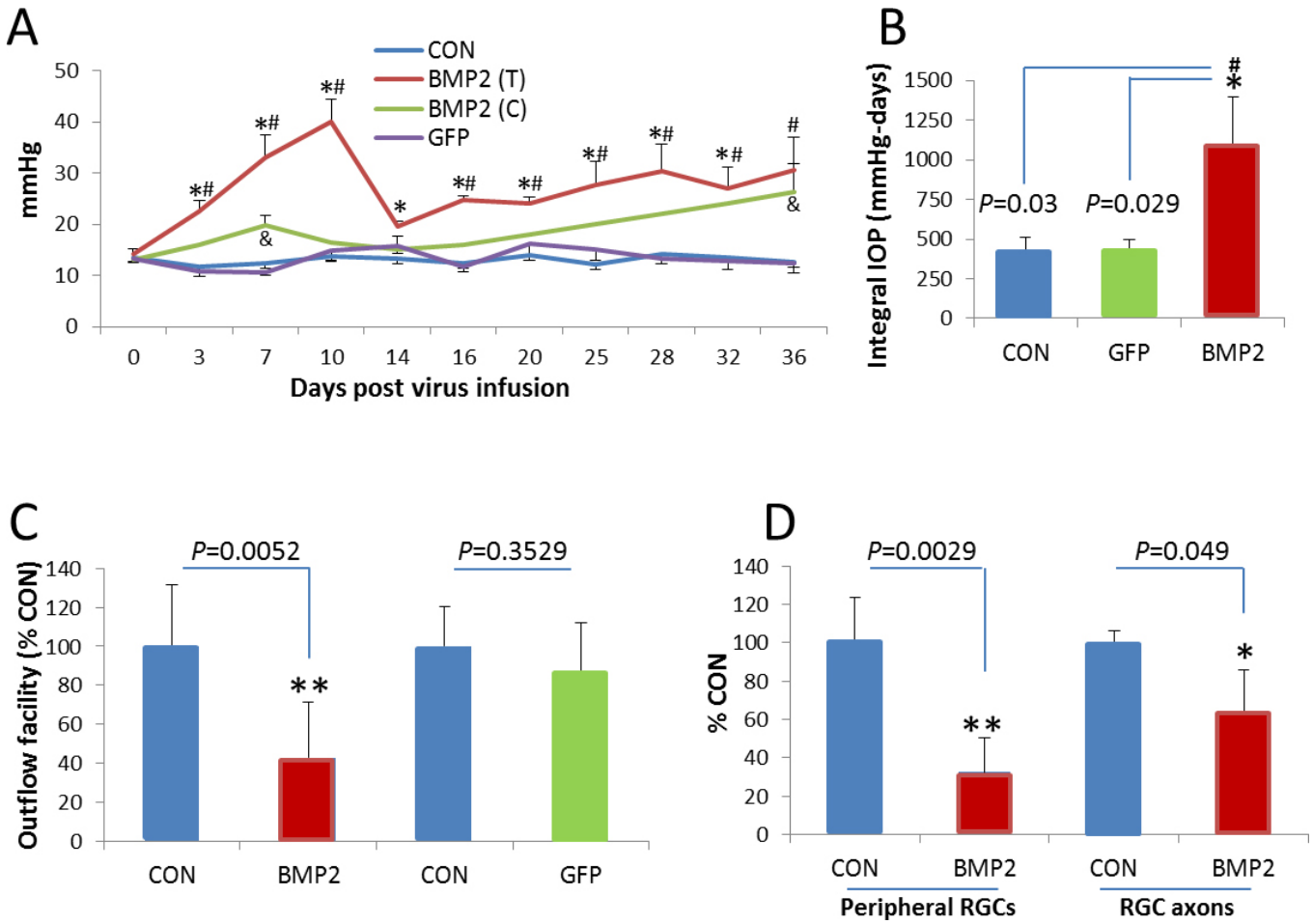

Figure 1. Characterization of the BMP2 mouse glaucoma model. **A**: Intraocular pressure (IOP) measurements over time from mice that transiently overexpress adenovirus-mediated BMP2 protein or green fluorescent protein (GFP) in iridocorneal angle tissues. Readings from TonoLab (T) and with direct cannulation (C) are compared to the untreated contralateral control eyes. **B**: Accumulated IOP insult is compared among the three groups over the 36-day measurement period. **C**: The outflow facility measurements in living mouse eyes that express BMP2 or GFP to the contralateral control eyes (CON) at 7 days post-viral infusion. **D**: IOP-mediated damage to retinal ganglion cells and myelinated axons in BMP2 mouse eyes at 36 days post-viral infusion. The IOP data represent mean ± SE; n=6 for the BMP2 eyes; n=6–12 for the GFP eyes. CON is cumulative data from the contralateral control eyes of the BMP2 and GFP infused mice (n=12–18); *p<0.05 comparing BMP2 eyes to contralateral controls; #p<0.05 comparing BMP2 to GFP eyes. Facility and RGC/axon data are mean ± SE, n=3–4, *p<0.05 comparing BMP2 to untreated contralateral control eyes.

in outflow tissues, and when the iridocorneal angle was open. As shown in Figure 1C, BMP2 overexpression significantly decreased outflow facility by 57.4% 7 days after the virus infusion compared to the contralateral control eye (non-transduced). In contrast, in the Ad.cmv.GFP infused eyes, outflow facility showed no difference from the contralateral eyes at 7 days post-transduction (Figure 1C).

To examine whether elevated IOP in BMP2-tranduced mouse eyes impacts RGC viability, we counted the number of RGC axons and cell bodies in the affected and unaffected contralateral eyes 36 days after the virus infusion. Using Brn3a labeling of RGC bodies of retinas in flatmounts, we observed a significant 68% decrease in peripheral RGC bodies in the BMP2 eyes compared to the contralateral controls (Figure 1D and Figure 3). Similarly, Figure 1D shows that there were significantly fewer myelinated axons in the optic nerves of the BMP2 mice compared to the contralateral control eyes.

Conventional outflow disease progression with standard histology: The BMP2-overexpressing mouse eyes were analyzed with light and electron microscopy. The eyes were examined at two key time points, 7 and 36 days after virus infusion. Results show that the peripheral cornea and the trabecular meshwork of BMP2 eyes were clearly thickened at

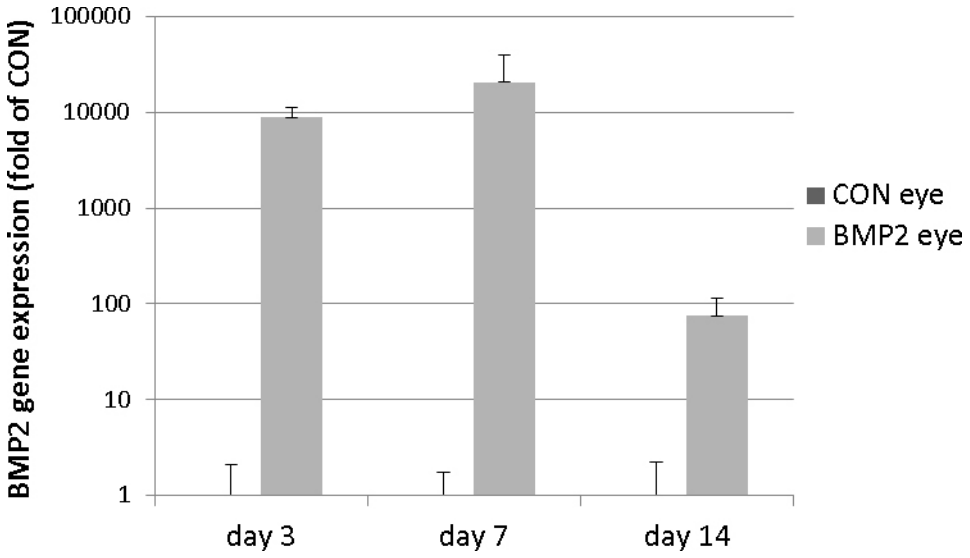

Figure 2. Human BMP2 RNA levels in mouse conventional outflow tissues. Adenovirus-encoding human BMP2 was infused intracamerally in the mouse eyes. At the indicated time points, the mouse outflow tissues (TM/SC) from the virus-infused eyes and the contralateral control eyes were dissected, and the total RNAs were isolated. The data show *BMP2* gene expression levels with quantitative real-time PCR normalized to the mouse β-actin mRNA. The data represent mean ± SD, N=3.

7 days post-transduction (Figure 4) compared to the contralateral control eyes and the GFP control eyes. Corneal thickness in the BMP2-transduced eyes returned to normal at 36 days, but the TM remained thickened, and the iridocorneal angle was completely closed (Figure 4). According to transmission electron microscopy, the BMP2 eyes contained increased collagen fibril content in the TM at 7 and 36 days (Figure 4).

BMP2-mediated conventional outflow disease progression with OCT: To determine whether morphological and functional changes in the conventional outflow pathway responsible for the elevated IOP and depressed outflow facility in the BMP2-transduced mice could be visualized over time, we used ultrahigh resolution OCT (0.9 µm axial). Figure 5 demonstrates that OCT imaging detected changes in the conventional outflow tissues over time, corresponding to the two phases of IOP elevation in the eyes that overexpressed BMP2. OCT showed that the iridocorneal angle of the BMP2 mouse eyes was open 7 days after transduction; however, the angle was narrower on day 10, and completely closed by day 23; the angle remained closed at all later time points (up to 90 days). Interestingly, the SC lumen was open, and was similar to the controls at all times checked. Similar to the standard histological methods, OCT also detected clear thickening of the peripheral cornea in the BMP2 eyes compared to the GFP eyes at days 7 and 10, returning to almost normal parameters

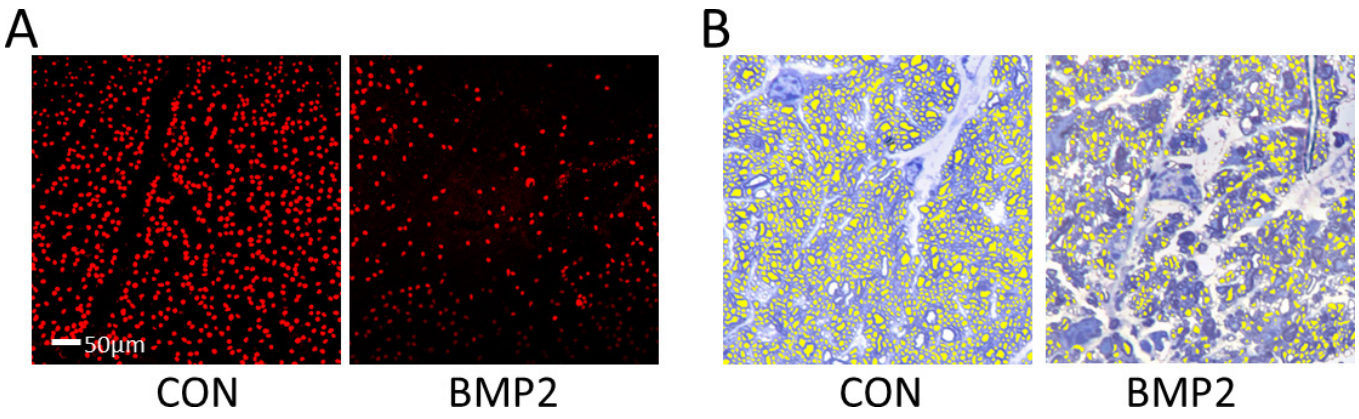

Figure 3. Assessment of damage to peripheral retinal ganglion cells and optic nerves in the mouse eyes that overexpressed BMP2 in conventional outflow tissues. Thirty-six days after the viral infusion, the mouse eyes and the optic nerves were collected. **A**: An image from the periphery of the flatmounted retinas of transduced mouse eyes that were immunostained with Brn3a immunoglobulin G (IgG) and imaged with epifluorescence microscopy. **B**: The morphology of the myelinated axons (toluidine blue stained) of mice 36 days after intracameral transduction with BMP2. The data are representative of images taken of four mice.

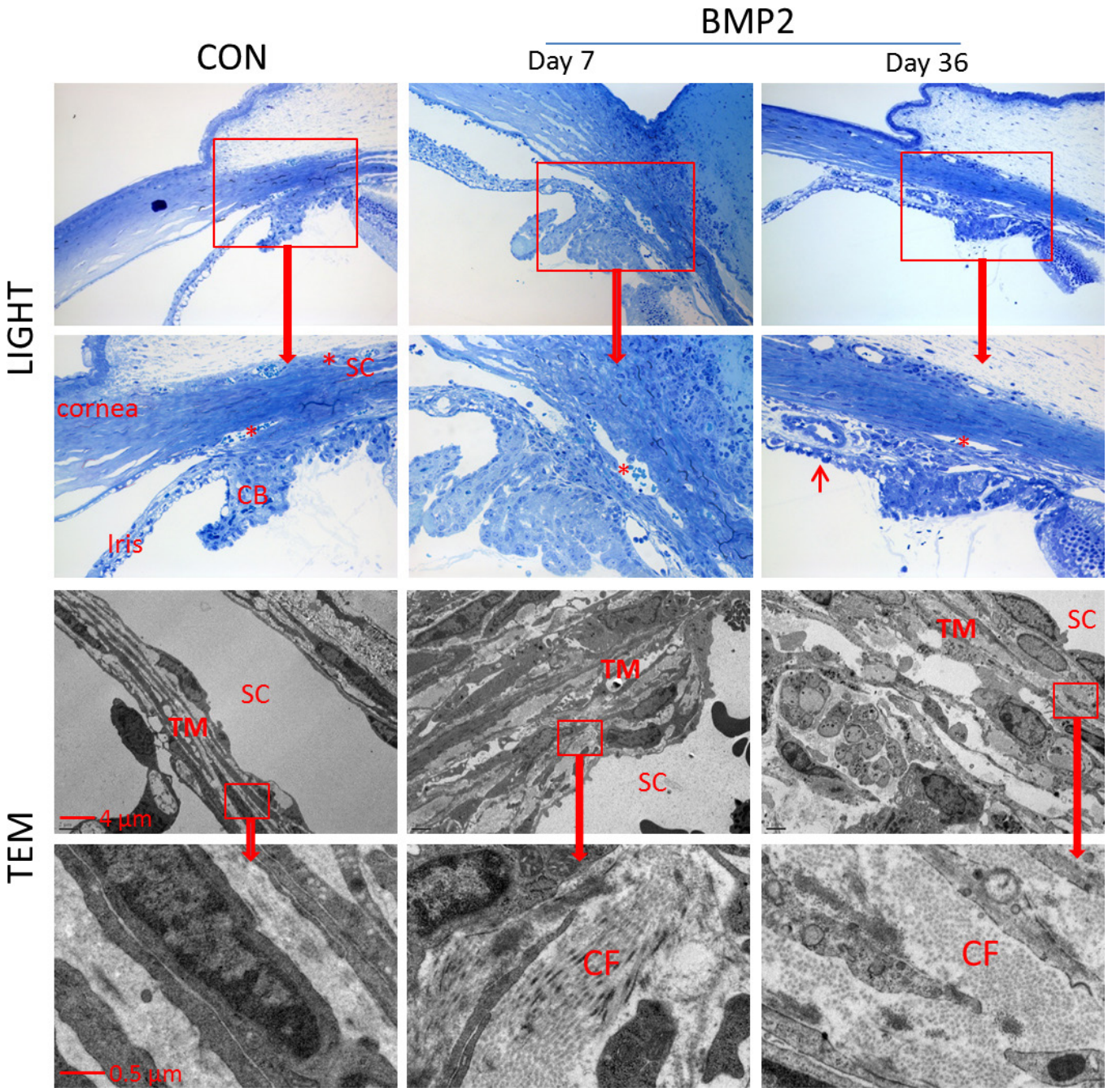

Figure 4. Morphological assessment of iridocorneal tissues of BMP2 mouse eyes with standard histological methods. Mouse eyes were fixed, and anterior segments (four quadrants) were processed for Epon embedding and sectioning (0.5 µm) at 7 and 36 days after Ad.cmv. BMP2 infusion. Sections were stained with 1% methylene blue, and images were captured digitally using light microscopy (top panels). The bottom panels show the ultrastructure of the mouse outflow tissues (65 nm sections stained with uranyl acetate/lead citrate) with transmission electron microscopy (TEM). The images are representative images of those taken from three mice in each group. Asterisk indicates the location of Schlemm's canal lumen; CB=ciliary body; CF=collagen fibrils; arrow points to iris synechiae (closed angle).

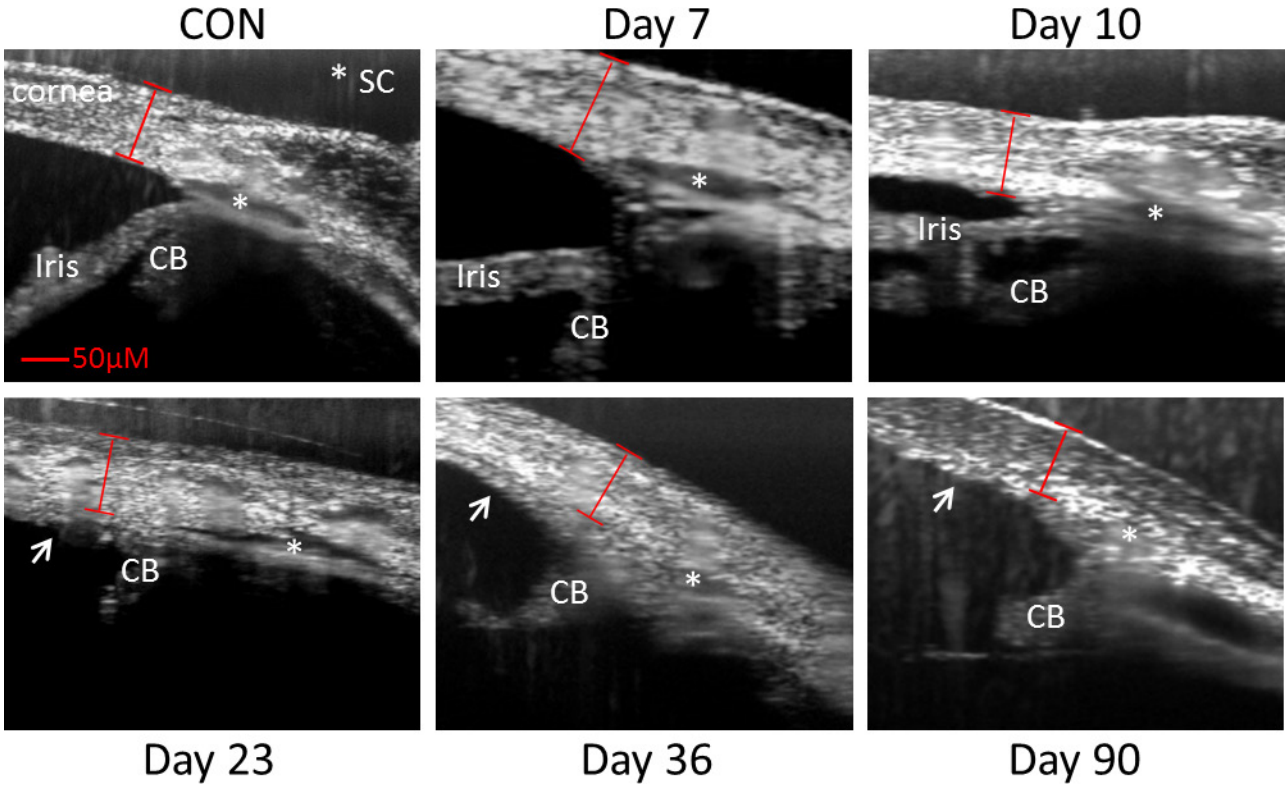

Figure 5. Monitoring disease progression of murine conventional outflow tissues overexpressing BMP2 using OCT. Shown are averaged intensity optimal coherence tomography (OCT) images of anterior angle tissues in the sagittal orientation 7, 10, 23, 36, or 90 days after infusion of adenovirus-encoding BMP2 or naive contralateral control (CON). All eyes were cannulated and held at 10 mmHg during the imaging sessions. A total of 14 mice were used in these experiments; representative data from one mouse (of three total) at each time point are shown. The exception is that only two mice were imaged at 90 days. Asterisk indicates the location of Schlemm's canal lumen; red brackets indicate peripheral corneal thickness; CB=ciliary body. The arrow shows iris synechiae (closed angle).

in the BMP2 eyes compared to the contralateral control eyes after 36 days.

Responses of conventional outflow tissues to IOP gradients visualized with OCT: We have recently shown that OCT resolves SC collapse caused by IOP elevation [25]. Here we investigated the impact of BMP2 or GFP overexpression on SC lumen dimensions in anesthetized mice with open iridocorneal angles and anterior chambers cannulated, and then challenged with sequential pressure gradients. Figure 6A shows that the SC lumen in the GFP and BMP2 transduced mouse eyes continued to decrease with sequential increases in IOP. Although we observed no significant differences between the GFP and BMP2 eyes at 7 days post-transduction, OCT showed significant differences in responses at day 10, and morphology and responses at 36 days post-transduction (Figure 6A). At 36 days, the SC lumen remained open during the IOP steps, and the angle remained closed. A summary of the analysis of the SC lumen area, comparing the BMP2 mice at 7, 10, and 36 days to the GFP control is shown in Figure 6B. We used the IOP versus SC lumen area relationship to roughly estimate the Young's modulus of the TM (E), a measure of tissue stiffness. Figure 7 shows an example of how the SC area was segmented on the OCT images. A summary of the stiffness estimates for the eyes only tested with open iridocorneal angles is shown in Table 1. For example, in the control eyes, E was 2.16 kPa, and there was a slight increase in E in eyes expressing GFP on day 7 but returned to near normal levels by day 36. In contrast, E increased by about 20% in the BMP2 eyes on day 7 and more than doubled on day 10 after transduction with the virus.

DISCUSSION

The present study showed for the first time that glaucomatous-like disease progression in a mouse can be assessed morphologically and functionally with OCT. Following intracameral gene delivery of human BMP2 to conventional outflow cells, a biphasic pattern in the outflow tissue morphology, stiffness, and IOP was observed over time. During the first phase, the trabecular meshwork and the cornea thickened, the

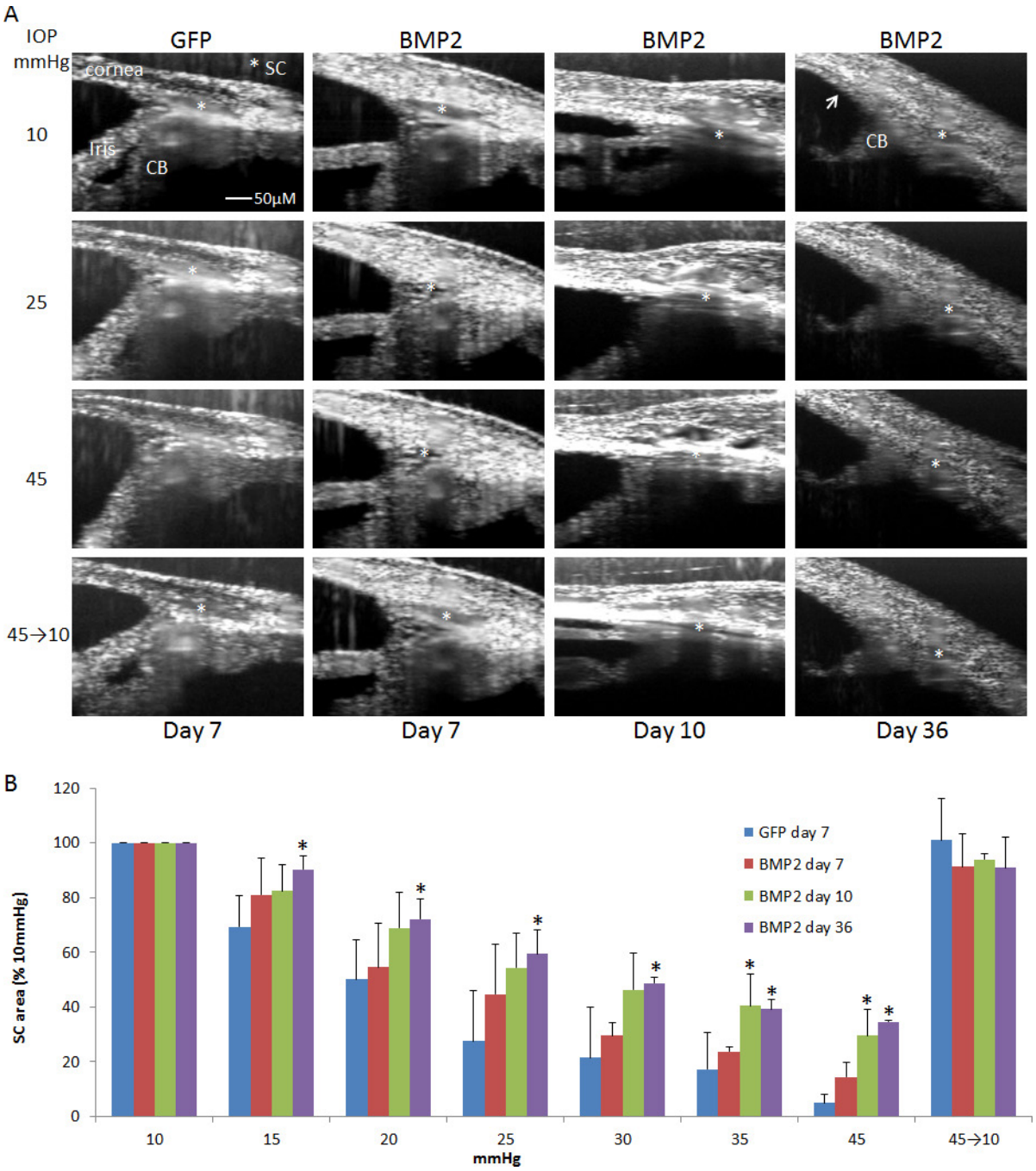

Figure 6. OCT imaging of conventional outflow tissues overexpressing BMP2 or GFP challenged with IOP gradients. After Ad.cmv.BMP2 or Ad.cmv.GFP infusion into one eye, the anesthetized mice were secured in a custom imaging platform. Eyes were cannulated with a glass needle to control and monitor intraocular pressure (IOP). The optical coherence tomography (OCT) probe was focused on an open Schlemm's canal (SC, asterisks), and images were captured at sequential IOPs of 10, 15, 20, 25, 30, 35, 45, and finally back to 10 mmHg. **A**: The averaged intensity images of the BMP2 mouse eyes subjected to four of these pressure steps over time compared to the control. Data shown were taken from different mice at each time point (representing a total of 12 that were imaged). CB=ciliary body. **B**: Quantitative analysis of Schlemm's canal lumen area in OCT images at sequential changes in cannulation-induced intraocular pressure. ImageJ software was used to analyze the OCT images captured from mice that were subjected to sequential changes in IOP as displayed in panel **A**. Data are normalized to the initial IOP of 10 mmHg to facilitate comparisons between animals, which had initial SC lumen dimensions that varied. Data represent mean ± SD, *p<0.05 comparing green fluorescent protein (GFP) and BMP2 eyes at 7, 10, and 36 days after viral infusion. All data are from mice with open iridocorneal angles, except BMP2 mice at 36 days, which had closed angles for comparisons.

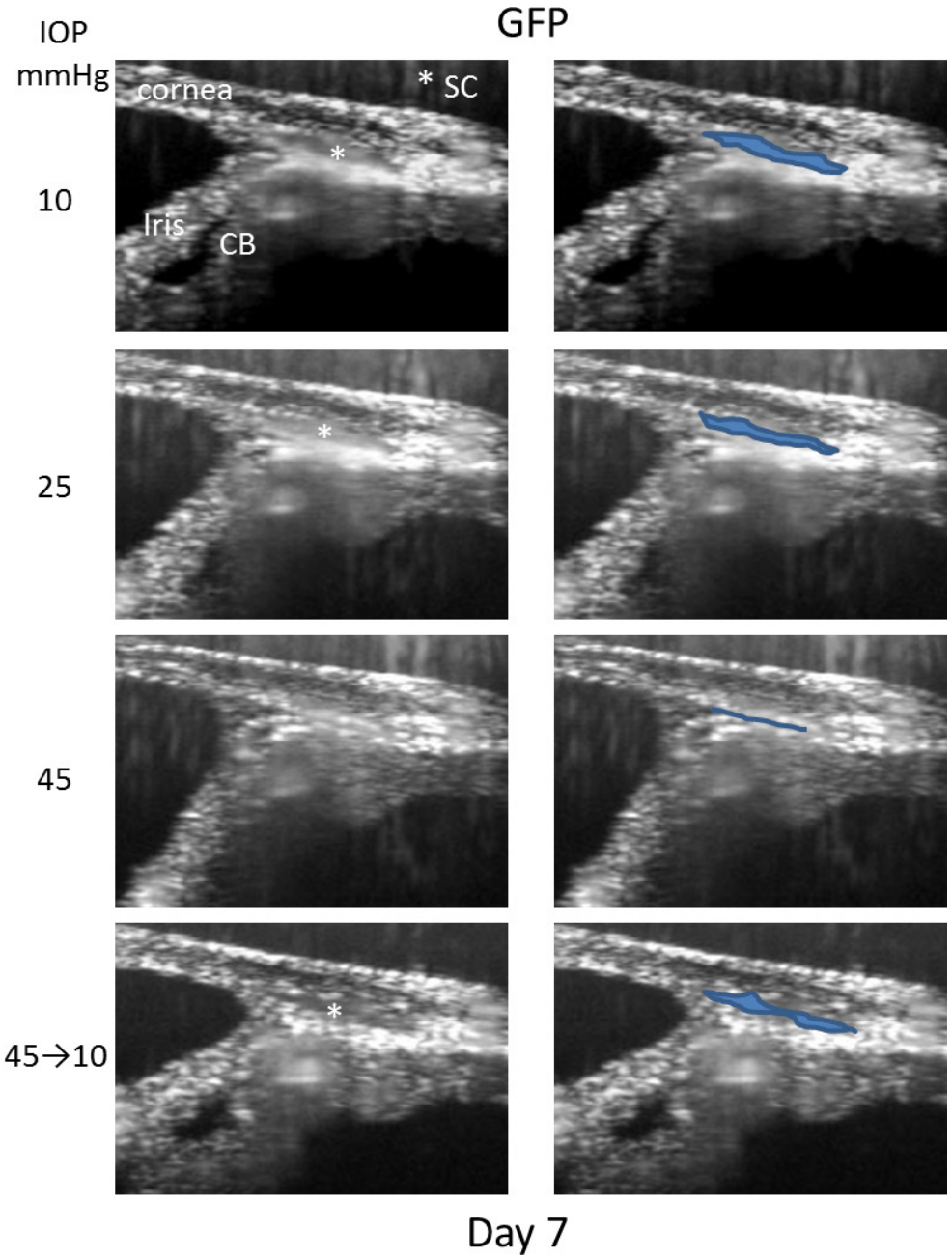

Figure 7. Example of SC lumen segmentation derived from OCT images of mouse eyes subjected to changes in IOP. In the left column are the average intensity images of the same region of a mouse anterior eye held sequentially at 10, 25, 45, and 10 mmHg. In the right column, the images are reproduced, and the SC lumen is outlined and highlighted. Asterisk shows the location of the SC lumen. CB=ciliary body. Images shown were obtained from one mouse out of a total of three control mice that were segmented.

iridocorneal angle was open, and the IOP and outflow tissue stiffness doubled, which lasted about 10 days. However, around day 14 the IOP decreased to nearly normal levels and remained lower for about a week. During this time interval, OCT revealed that the iridocorneal angle began to close, with complete anterior synechia by day 23 when the IOP began to rise again. The IOP remained elevated and the iridocorneal angle closed for all subsequent measurements. Thus, BMP2 overexpression mediates pathophysiological changes in the conventional outflow tissues of mice that resulted first in open-angle ocular hypertension and then progressing to angle-closure glaucoma.

In the posterior eye, OCT has been used in the clinic to identify stages of punctate inner choroidopathy [37] and short-term changes in basal laminar drusen in age-related macular degeneration [38] in human eyes. OCT has also been used to follow changes in the optic nerve head [39] and the retina nerve fiber layer thickness [40] in experimental glaucoma induced in monkey eyes. In the anterior eye, OCT has been used to detect spontaneous deflation of an iris pigment

Table 1. Estimated Young's modulus (E) of TM in CD1 mouse eyes overexpressing BMP2 or GFP.

Mouse	IOP	100/E (mmHg)	E (kPa)
Naive Control	13.15±2.27	6.16	2.16
GFP/7 days	10.69±2.66	4.74	2.82
BMP2/7 days	19.7±2.1	3.86	3.46
BMP2/10 days	24.3±4.8	2.66	5.01
GFP/36 days	12.44±4.38	6.06	2.20

IOP: intraocular pressure

epithelial cyst in a case report [41]. OCT also followed progressive corneal edema in a transgenic mouse model of a congenital hereditary endothelial dystrophy [42]. However, to our knowledge, this is the first study to follow progressive changes in iridocorneal angle tissues in a mouse model of glaucoma with OCT.

Using a custom mouse holder equipped with a micromanipulator, we simultaneously changed the IOP and monitored the effects on conventional outflow structures using OCT to derive information about TM stiffness. We observed that SC was more resistant to collapse in the eyes that overexpressed BMP2 versus GFP. These data are consistent with our previous findings that showed increased resistance of SC to collapse in mouse eyes treated with pilocarpine [25]. In the previous study, increased stiffness in the TM was caused by the tension created on the TM through ciliary muscle contraction. In the present study, it appeared that increased stiffness was the result of BMP2-mediated changes in the extracellular matrix of the TM. Stiffness of the TM can be detected with atomic force microscopy in human donor eyes [43], but not currently in mouse eyes due to technical difficulties (smaller tissues and thinner TM layer). However, using a previous published method [36], we estimated the stiffness of the mouse TM by measuring the SC collapse following changes in the pressure difference across the TM. Importantly, we resolved differences between the GFP and BMP2 overexpressing TMs (in eyes with open iridocorneal angles) using this method. Interestingly, our measurements of the TM stiffness in the mouse are comparable (2–5 kPa) with direct atomic force microscopy (AFM) measurements of human TM from non-glaucomatous cadaveric eyes [43].

BMP2 belongs to the BMP family of proteins, part of the TGFβ superfamily [44-46]. Similar to TGFβ2-mediated increases in extracellular matrix accumulation, we found extensive extracellular matrix deposition in the TM of the BMP2 transduced eyes, making the TM much thicker than normal. Transmission electron microscopy showed that the thickened TM was in part due to a dramatic increase in the number of collagen fibrils present in the TM. It has been shown previously that overexpression of BMP2 by trabecular meshwork cells in culture induces collagen type I alpha 1 mRNA expression at a level 41-fold over untreated cells [29]. Thus, the TM appears fibrotic following BMP2 overexpression, consistent with the stiffness increase observed in this study.

OCT of living mouse eyes that overexpressed BMP2 also detected early swelling of the cornea. This observation motivated us to reevaluate the IOP using a direct method, in addition to rebound tonometry, which relies on corneal properties to accurately estimate the IOP. A direct measurement of the IOP with cannulation of the anterior chamber was used to determine the impact of corneal swelling on the tonometry measurements. Although the IOP was clearly elevated and biphasic over time in the BMP2 mice, tonometry overestimated the IOP during the first phase of the disease procession. In contrast, the pressure data from both methods were similar during phase 2, consistent with the corneal thickness returning to normal. Cornea edema and thickness in phase 1 may be induced by the acute elevation of the IOP [47-49] and/or by overexpression of BMP2 in the peripheral corneal endothelial cells. Thus, BMP2 overexpression may provoke the immune system, similar to other members of the TGFβ family [50,51]. With transmission electron microscopy, we observed immune cells in the TM of the BMP2 transduced mouse eyes (not shown), similar to findings in other model systems [50]. In addition, TM pathology may in part be mediated by immune responses to viral vectors; however, the GFP transduced eyes appear indistinguishable from the non-transduced controls.

The present study extended work reported recently showing that BMP2 overexpression in rat eyes results in ocular hypertension [29]. This study also used adenovirus as a gene delivery vehicle, subjecting rats to a virus load similar to the present study. Results of BMP2 overexpression in rats showed that the IOP started to increase at 7 days post-injection, about two to three times that of the control eyes, and

remained elevated for 48 days measured with either TonoLab or Tono-Pen. In comparison, in the present study, the IOP in the BMP2 mouse eyes was elevated within 2–3 days post-infusion, and the highest level was about three times over the control eyes according to TonoLab. Although corneal opacity was reported in about 30% of the BMP2 rat eyes, gross changes in the iridocorneal angle and the TM were not detected; however, light microscopy revealed increased abundance of the extracellular matrix in some of the TMs in the BMP2 rats after 76 days. In the present study, we did not observe corneal opacity but peripheral corneal edema, which occurred in all of the mice. By 29 days after the BMP2 virus injection in rat eyes, about 34% of peripheral RGCs were lost compared to null virus. In contrast, at 36 days post-viral infusion, we observed 68% of peripheral RGCs and about 36% of the myelinated axons were lost in the mouse eyes that overexpressed BMP2. This is compared to the approximate 20% axon loss for the bead glaucoma model in C57/BL6 mice [52], which are less susceptible to damage [6]. Unlike mice, the iridocorneal angle of BMP2 rats does not close at later time points. Also different in the present study was the use of OCT, transmission electron microscopy, IOP measured with direct cannulation of anterior chamber, and outflow facility measurements in BMP2 mice.

OCT is a valuable tool and routinely used in the clinic for detecting and managing ocular diseases because of the noncontact, noninvasive, real time, and non-toxic features. OCT has been used to determine the stages of angle closure in closed-angle glaucoma [53,54]. OCT was also used to show that SC is smaller in eyes with primary open-angle glaucoma (POAG) compared to normal control eyes [24,55]. However, POAG has many subtypes, and glaucomatous eyes show a spectrum of responses to treatments. Our study successfully visualized changes, both morphological and functional, in conventional outflow tissues of mice transduced with BMP2. This BMP2-induced mouse ocular hypertension model provides the first proof of concept that OCT has the potential to detect early changes in the conventional outflow pathway in those with ocular hypertensive glaucoma and to follow disease progression and treatment efficacy.

ACKNOWLEDGEMENTS

The authors thank Ying Hao for help with histology. This study was funded by the National Eye Institute (EY023287) and the Research to Prevent Blindness Foundation.

REFERENCES

1. WoldeMussie E, Ruiz G, Wijono M, Wheeler LA. Neuroprotection of retinal ganglion cells by brimonidine in rats with laser-induced chronic ocular hypertension Invest Ophthalmol Vis Sci 2001; 42:2849-55. [PMID: 11687528].
2. Garcia-Valenzuela E, Shareef S, Walsh J, Sharma SC. Programmed cell death of retinal ganglion cells during experimental glaucoma Exp Eye Res 1995; 61:33-44. [PMID: 7556468].
3. Morrison JC, Moore CG, Deppmeier LM, Gold BG, Meshul CK, Johnson EC. A rat model of chronic pressure-induced optic nerve damage Exp Eye Res 1997; 64:85-96. [PMID: 9093024].
4. Mabuchi F, Aihara M, Mackey MR, Lindsey JD, Weinreb RN. Optic nerve damage in experimental mouse ocular hypertension Invest Ophthalmol Vis Sci 2003; 44:4321-30. [PMID: 14507876].
5. Ruiz-Ederra J, Verkman AS. Mouse model of sustained elevation in intraocular pressure produced by episcleral vein occlusion Exp Eye Res 2006; 82:879-84. [PMID: 16310189].
6. Cone FE, Gelman SE, Son JL, Pease ME, Quigley HA. Differential susceptibility to experimental glaucoma among 3 mouse strains using bead and viscoelastic injection Exp Eye Res 2010; 91:415-24. [PMID: 20599961].
7. Cone FE, Steinhart MR, Oglesby EN, Kalesnykas G, Pease ME, Quigley HA. The effects of anesthesia, mouse strain and age on intraocular pressure and an improved murine model of experimental glaucoma Exp Eye Res 2012; 99:27-35. [PMID: 22554836].
8. Kipfer-Kauer A, McKinnon SJ, Frueh BE, Goldblum D. Distribution of amyloid precursor protein and amyloid-beta in ocular hypertensive C57BL/6 mouse eyes Curr Eye Res 2010; 35:828-34. [PMID: 20795865].
9. Libby RT, Li Y, Savinova OV, Barter J, Smith RS, Nickells RW, John SW. Susceptibility to neurodegeneration in a glaucoma is modified by Bax gene dosage PLoS Genet 2005; 1:17-26. [PMID: 16103918].
10. Howell GR, Soto I, Ryan M, Graham LC, Smith RS, John SW. Deficiency of complement component 5 ameliorates glaucoma in DBA/2J mice J Neuroinflammation 2013; 10:76-[PMID: 23806181].
11. Howell GR, Macalinao DG, Sousa GL, Walden M, Soto I, Kneeland SC, Barbay JM, King BL, Marchant JK, Hibbs M, Stevens B, Barres BA, Clark AF, Libby RT, John SW. Molecular clustering identifies complement and endothelin induction as early events in a mouse model of glaucoma J Clin Invest 2011; 121:1429-44. [PMID: 21383504].
12. Senatorov V, Malyukova I, Fariss R, Wawrousek EF, Swaminathan S, Sharan SK, Tomarev S. Expression of mutated mouse myocilin induces open-angle glaucoma in transgenic mice. J Neurosci 2006; 26:11903-14. [PMID: 17108164].
13. McDowell CM, Luan T, Zhang Z, Putliwala T, Wordinger RJ, Millar JC, John SW, Pang IH, Clark AF. Mutant human myocilin induces strain specific differences in ocular

hypertension and optic nerve damage in mice Exp Eye Res 2012; 100:65-72. [PMID: 22575566].

14. Junglas B, Kuespert S, Seleem AA, Struller T, Ullmann S, Bosl M, Bosserhoff A, Kostler J, Wagner R, Tamm ER, Fuchshofer R. Connective tissue growth factor causes glaucoma by modifying the actin cytoskeleton of the trabecular meshwork Am J Pathol 2012; 180:2386-403. [PMID: 22542845].
15. Aihara M, Lindsey JD, Weinreb RN. Ocular hypertension in mice with a targeted type I collagen mutation Invest Ophthalmol Vis Sci 2003; 44:1581-5. [PMID: 12657595].
16. Shepard AR, Millar JC, Pang IH, Jacobson N, Wang WH, Clark AF. Adenoviral gene transfer of active human transforming growth factor-{beta}2 elevates intraocular pressure and reduces outflow facility in rodent eyes Invest Ophthalmol Vis Sci 2010; 51:2067-76. [PMID: 19959644].
17. Dai Y, Lindsey JD, Duong-Polk X, Nguyen D, Hofer A, Weinreb RN. Outflow facility in mice with a targeted type I collagen mutation Invest Ophthalmol Vis Sci 2009; 50:5749-53. [PMID: 19797236].
18. Huang D, Swanson EA, Lin CP, Schuman JS, Stinson WG, Chang W, Hee MR, Flotte T, Gregory K, Puliafito CA, Fujimoto JG. Optical coherence tomography. Science 1991; 254:1178-81. [PMID: 1957169].
19. Hee MR, Izatt JA, Swanson EA, Huang D, Schuman JS, Lin CP, Puliafito CA, Fujimoto JG. Optical coherence tomography of the human retina Arch Ophthalmol 1995; 113:325-32. [PMID: 7887846].
20. Srinivasan PP, Heflin SJ, Izatt JA, Arshavsky VY, Farsiu S. Automatic segmentation of up to ten layer boundaries in SD-OCT images of the mouse retina with and without missing layers due to pathology Biomed Opt Express 2014; 5:348-65. [PMID: 24575332].
21. Kagemann L, Wollstein G, Ishikawa H, Sigal IA, Folio LS, Xu J, Gong H, Schuman JS. 3D visualization of aqueous humor outflow structures in-situ in humans Exp Eye Res 2011; 93:308-15. [PMID: 21514296].
22. Usui T, Tomidokoro A, Mishima K, Mataki N, Mayama C, Honda N, Amano S, Araie M. Identification of Schlemm's Canal and Its Surrounding Tissues by Anterior Segment Fourier Domain Optical Coherence Tomography Invest Ophthalmol Vis Sci 2011; 52:6934-9. [PMID: 21757587].
23. Leung CKS, Weinreb RN. Anterior chamber angle imaging with optical coherence tomography Eye (Lond) 2011; 25:261-7. [PMID: 21242985].
24. Kagemann L, Wollstein G, Ishikawa H, Nadler Z, Sigal IA, Folio LS, Schuman JS. Visualization of the conventional outflow pathway in the living human eye Ophthalmology 2012; 119:1563-8. [PMID: 22683063].
25. Li G, Farsiu S, Chiu SJ, Gonzalez P, Lutjen-Drecoll E, Overby DR, Stamer WD. Pilocarpine-induced dilation of Schlemm's canal and prevention of lumen collapse at elevated intraocular pressures in living mice visualized by OCT Invest Ophthalmol Vis Sci 2014; 55:3737-46. [PMID: 24595384].
26. Sampath TK, Coughlin JE, Whetstone RM, Banach D, Corbett C, Ridge RJ, Ozkaynak E, Oppermann H, Rueger DC. Bovine osteogenic protein is composed of dimers of OP-1 and BMP-2A, two members of the transforming growth factor-beta superfamily J Biol Chem 1990; 265:13198-205. [PMID: 2376592].
27. Wordinger RJ, Sharma T, Clark AF. The role of TGF-β2 and bone morphogenetic proteins in the trabecular meshwork and glaucoma. J Ocul Pharmacol Ther 2014; 30:154-62. [PMID: 24517218].
28. Xue W, Wallin R, Olmsted-Davis EA, Borras T. Matrix GLA protein function in human trabecular meshwork cells: inhibition of BMP2-induced calcification process Invest Ophthalmol Vis Sci 2006; 47:997-1007. [PMID: 16505034].
29. Buie LK, Karim MZ, Smith MH, Borras T. Development of a model of elevated intraocular pressure in rats by gene transfer of bone morphogenetic protein 2 Invest Ophthalmol Vis Sci 2013; 54:5441-55. [PMID: 23821199].
30. Thévenaz P, Ruttimann UE, Unser M. A pyramid approach to subpixel registration based on intensity. IEEE Trans Image Process 1998; 7:27-41. [PMID: 18267377].
31. Li G, Gonzalez P, Camras LJ, Navarro I, Qiu J, Challa P, Stamer WD. Optimizing gene transfer to conventional outflow cells in living mouse eyes Exp Eye Res 2013; 109:8-16. [PMID: 23337742].
32. Hodneland E, Kogel T, Frei D, Gerdes H-H, Lundervold A. CellSegm - a MATLAB toolbox for high-throughput 3D cell segmentation Source Code Biol Med 2013; 8:16-[PMID: 23938087].
33. McKinnon SJ, Lehman DM, Tahzib NG, Ransom NL, Reitsamer HA, Liston P, LaCasse E, Li Q, Korneluk RG, Hauswirth WW. Baculoviral IAP repeat-containing-4 protects optic nerve axons in a rat glaucoma model. Mol Ther 2002; 5:780-7. [PMID: 12027563].
34. Camras LJ, Sufficool KE, Camras CB, Fan S, Liu H, Toris CB. Duration of anesthesia affects intraocular pressure, but not outflow facility in mice Curr Eye Res 2010; 35:819-27. [PMID: 20795864].
35. Kagemann L, Wang B, Wollstein G, Ishikawa H, Nevins JE, Nadler Z, Sigal IA, Bilonick RA, Schuman JS. IOP elevation reduces Schlemm's canal cross-sectional area Invest Ophthalmol Vis Sci 2014; 55:1805-9. [PMID: 24526436].
36. Johnson MC, Kamm RD. The role of Schlemm's canal in aqueous outflow from the human eye Invest Ophthalmol Vis Sci 1983; 24:320-5. [PMID: 6832907].
37. Zhang X, Zuo C, Li M, Chen H, Huang S, Wen F. Spectral-domain optical coherence tomographic findings at each stage of punctate inner choroidopathy Ophthalmology 2013; 120:2678-83. [PMID: 23769333].
38. van de Ven JP, Boon CJ, Smailhodzic D, Lechanteur YT, den Hollander AI, Hoyng CB, Theelen T. Short-term changes of Basal laminar drusen on spectral-domain optical coherence tomography Am J Ophthalmol 2012; 154:560-7. [PMID: 22626619].

39. Strouthidis NG, Fortune B, Yang H, Sigal IA, Burgoyne CF. Longitudinal change detected by spectral domain optical coherence tomography in the optic nerve head and peripapillary retina in experimental glaucoma Invest Ophthalmol Vis Sci 2011; 52:1206-19. [PMID: 21217108].

40. Schuman JS, Pedut-Kloizman T, Pakter H, Wang N, Guedes V, Huang L, Pieroth L, Scott W, Hee MR, Fujimoto JG, Ishikawa H, Bilonick RA, Kagemann L, Wollstein G. Optical coherence tomography and histologic measurements of nerve fiber layer thickness in normal and glaucomatous monkey eyes Invest Ophthalmol Vis Sci 2007; 48:3645-54. [PMID: 17652734].

41. Kytasty C, Parvus BJ, Mahmood Z, Shields CL, Shields JA. Spontaneous deflation of an iris pigment epithelial cyst documented with AS-OCT. Ophthalmic Surg Lasers Imaging 2010; 41:e1-3. [PMID: 21053866].

42. Han SB, Ang HP, Poh R, Chaurasia SS, Peh G, Liu J, Tan DT, Vithana EN, Mehta JS. Mice with a targeted disruption of Slc4a11 model the progressive corneal changes of congenital hereditary endothelial dystrophy Invest Ophthalmol Vis Sci 2013; 54:6179-89. [PMID: 23942972].

43. Last JA, Pan T, Ding Y, Reilly CM, Keller K, Acott TS, Fautsch MP, Murphy CJ, Russell P. Elastic modulus determination of normal and glaucomatous human trabecular meshwork Invest Ophthalmol Vis Sci 2011; 52:2147-52. [PMID: 21220561].

44. Helbing T, Herold EM, Hornstein A, Wintrich S, Heinke J, Grundmann S, Patterson C, Bode C, Moser M. Inhibition of BMP activity protects epithelial barrier function in lung injury J Pathol 2013; 231:105-16. [PMID: 23716395].

45. McCormack N, Molloy EL, O'Dea S. Bone morphogenetic proteins enhance an epithelial-mesenchymal transition in normal airway epithelial cells during restitution of a disrupted epithelium Respir Res 2013; 14:36-[PMID: 23509993].

46. Wordinger RJ, Agarwal R, Talati M, Fuller J, Lambert W, Clark AF. Expression of bone morphogenetic proteins (BMP), BMP receptors, and BMP associated proteins in human trabecular meshwork and optic nerve head cells and tissues Mol Vis 2002; 8:241-50. [PMID: 12131877].

47. Olsen T. The endothelial cell damage in acute glaucoma. On the corneal thickness response to intraocular pressure Acta Ophthalmol (Copenh) 1980; 58:257-66. [PMID: 7395487].

48. Chen MJ, Liu CJ, Cheng CY, Lee SM. Corneal status in primary angle-closure glaucoma with a history of acute attack J Glaucoma 2012; 21:12-6. [PMID: 21048505].

49. Sihota R, Lakshmaiah NC, Titiyal JS, Dada T, Agarwal HC. Corneal endothelial status in the subtypes of primary angle closure glaucoma Clin Experiment Ophthalmol 2003; 31:492-5. [PMID: 14641156].

50. Shen J, James AW, Zara JN, Asatrian G, Khadarian K, Zhang JB, Ho S, Kim HJ, Ting K, Soo C. BMP2-induced inflammation can be suppressed by the osteoinductive growth factor NELL-1 Tissue Eng Part A 2013; 19:2390-401. [PMID: 23758588].

51. Ara J, See J, Mamontov P, Hahn A, Bannerman P, Pleasure D, Grinspan JB. Bone morphogenetic proteins 4, 6, and 7 are up-regulated in mouse spinal cord during experimental autoimmune encephalomyelitis J Neurosci Res 2008; 86:125-35. [PMID: 17722066].

52. Sappington RM, Carlson BJ, Crish SD, Calkins DJ. The microbead occlusion model: a paradigm for induced ocular hypertension in rats and mice Invest Ophthalmol Vis Sci 2010; 51:207-16. [PMID: 19850836].

53. Moghimi S, Zandvakil N, Vahedian Z, Mohammadi M, Fakhraie G, Coleman AL, Lin SC. Acute angle closure: qualitative and quantitative evaluation of the anterior segment using anterior segment optical coherence tomography Clin Experiment Ophthalmol 2014; [PMID: 24330237].

54. Nongpiur ME, Haaland BA, Perera SA, Friedman DS. He M5, Sakata LM, Baskaran M3, Aung T. Development of a score and probability estimate for detecting angle closure based on anterior segment optical coherence tomography. Am J Ophthalmol 2014; 157:32-8. [PMID: 24210768].

55. Hong J, Xu J, Wei A, Wen W, Chen J, Yu X, Sun X. Spectral-domain optical coherence tomographic assessment of Schlemm's canal in Chinese subjects with primary open-angle glaucoma Ophthalmology 2013; 120:709-15. [PMID: 23352198].

Articles are provided courtesy of Emory University and the Zhongshan Ophthalmic Center, Sun Yat-sen University, P.R. China. The print version of this article was created on 20 December 2014. This reflects all typographical corrections and errata to the article through that date. Details of any changes may be found in the online version of the article.